Available online at www.sciencedirect.com
SCIENCE DIRECT®
ELSEVIER
International Journal of Solids and Structures 43 (2006) 4867–4887
INTERNATIONAL JOURNAL OF SOLIDS and STRUCTURES
www.elsevier.com/locate/ijsolstr

Large displacement analysis of elastic pyramidal trusses

S.S. Ligarò *, P.S. Valvo

Department of Structural Engineering, University of Pisa, Via Diotisalvi 2, I-56126 Pisa, Italy

Received 7 April 2005; received in revised form 28 June 2005
Available online 8 September 2005

Abstract

The paper examines the equilibrium stability problem for a simple class of elastic space trusses in the shape of a regular pyramid. Joints located at the vertices of the base polygon are fixed while the joint at the apex is subjected to a proportionally increasing load acting in either the vertical direction, in the horizontal plane, or along a generic oblique direction. Exact closed-form solutions are derived for each load condition under the common hypotheses of linear material law, small or moderate axial deformation in bars and large nodal displacements. Despite their seeming simplicity, these mechanical systems exhibit a wide variety of post-critical responses, not exhausted by the classical snapping and bifurcation phenomena. In addition to regular primary and secondary branches, the equilibrium paths may include neutral branches, namely branches entirely composed of bifurcation or limit points. Besides their immediate theoretical interest, these branches are particularly difficult to handle by the standard numerical procedures of non-linear analysis, so the given solutions may represent severe benchmark tests.

Keywords: Space trusses; Elastic stability; Large displacement analysis; Equilibrium paths; Snap-through; Bifurcation; Neutral branches

1. Introduction

The shallow symmetric two-bar planar truss depicted in Fig. 1a, subjected to a vertical load at its top joint, is no doubt the most popular example of a structural system where snap-through is the prevailing form of instability. It is currently associated to the name of von Mises (1923, 1925), who first used this model to explore kinds of structural instability more general than Euler's buckling of a single bar. However, it would be unfair to relate this scheme to the snap-through phenomenon only. In fact, as clearly highlighted

* Corresponding author. Tel.: +39 050 835711; fax: +39 050 554597.
E-mail addresses: s.ligaro@ing.unipi.it (S.S. Ligarò), p.valvo@ing.unipi.it (P.S. Valvo).

0020-7683/$ - see front matter © 2005 Elsevier Ltd. All rights reserved.
doi:10.1016/j.ijsolstr.2005.06.100

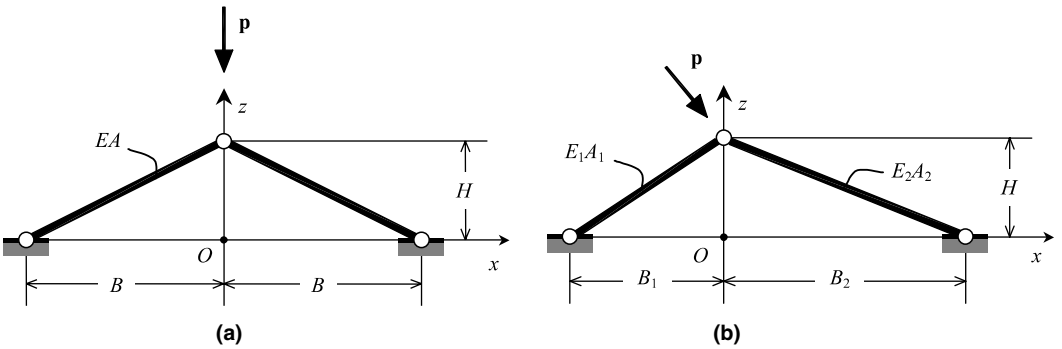

Fig. 1. The two-bar planar truss: (a) symmetric case, (b) general case.

by Pecknold et al. (1985), significant changes in the structural response can be obtained by introducing some slight modifications to the static scheme or to the load pattern. Thus, for instance, if the height to base ratio of the truss, H/B, is increased (and the hypothesis of symmetry is released), the two-bar planar truss may exhibit a bifurcation instability. Moreover, if a linear elastic spring is placed along the symmetry axis, then a strain-hardening behaviour emerges in the post-critical response, but, if a perturbing horizontal load is added to the vertical one, then bifurcation points change into (more or less sharp) turning points. The latter result is not surprising, if we consider that the horizontal load is to all intents an imperfection in the sense of Koiter (1976). In this case, the symmetry of the model is lost, and its post-critical behaviour becomes a combination of those exhibited by the perfect system when a vertical load or a horizontal one acts separately. When a geometrical imperfection is considered, the equilibrium path is composed of primary and secondary branches not connected to each other (for the closed-form solution of the asymmetric two-bar truss of Fig. 1b, see Ligarò and Valvo, 1999). Finally, further modifications to the original scheme were independently introduced by Crisfield (1991) and by Bazant and Cedolin (1991) to reproduce more involved types of structural instabilities such as snap-back.

Unlike the two-dimensional case, when dealing with stability problems of space structures, the lack of closed-form solutions, even in cases of particularly simple spatial systems, constitutes a serious gap, so that, recourse to numerical procedures of non-linear analysis, notwithstanding their degree of sophistication, always remains accompanied by a halo of uncertainty.

This paper is concerned with the large displacement analysis of a class of elastic space trusses in the shape of a regular pyramid. These structures represent the simplest three-dimensional generalisation of the 'perfect' two-bar system mentioned above. Pyramidal trusses possess an immediate practical interest since they are currently used in many present-day civil constructions, either as main parts or as minor elements. For instance, if the number n of the composing bars is 3, we find a common tripod-like structure loaded on its upper joint. For $n = 4$ and a large height to base ratio, the truss may represent the cap of a mast or, if the load acts transversally, the extremity of a three-dimensional cantilever beam or of the jib of a tower crane. Finally, for $n = 5$ or $n = 6$ and a small height to base ratio, the truss may schematise a molecule of a single-layer geodesic dome or of a generic-shaped reticulated shell.

The paper is organised as follows: in Section 2, a complete description of the mechanical model and the system of loads is given. Assuming the latter to be conservative, the governing set of the non-linear equilibrium equations is obtained by recourse to the principle of stationary total potential energy. Section 3 analyses the conditions for the existence of stable equilibrium configurations. Regions of the coordinate space associated with stable equilibrium states are determined and conditions are discussed for which bifurcation and/or snapping instability may occur. Section 4 is dedicated to the search for those configurations where the system is in equilibrium in absence of any applied load. As a result, kinematic paths and states of

self-stress are determined at the same time. Knowledge of the above configurations is of great importance in stability analysis, since they constitute points of obligatory passage for the equilibrium paths associated with any reference load vector. In Section 5, the non-linear equilibrium problem is solved with reference to three different loading conditions: first, we consider a proportional vertical load acting on the top joint, then we analyse the case of a horizontal load and, finally, we consider a load acting along a generic oblique direction. The analytical expressions of the equilibrium paths (primary and complementary branches) are given in closed-form for all the aforementioned cases. Finally, some concluding remarks are given in Section 6.

2. Formulation of the problem

Let us consider a space truss made of $n \geqslant 3$ identical elastic bars, which in the *reference configuration* C_0 are placed along the lateral edges of a regular pyramid (Fig. 2a). Let H be the height of the pyramid, B the radius of the circle Γ which circumscribes the base polygon and $L = \sqrt{H^2 + B^2}$ the length of the bars.

The apex joint is assumed to be free to move and subjected to a load $\lambda\mathbf{p}$, where $\lambda \in (-\infty, +\infty)$ is a real multiplier and $\mathbf{p} = [p_x, p_y, p_z]^{\mathrm{T}}$ is a *reference load vector* (the superscript T denotes the transposition). Joints located at the base vertices, identified in counter-clockwise order by the integers $1,2,\ldots,n$, are fixed at rest. All joints behave as ideal frictionless hinges, so bars are subjected to axial forces only.

The bars are made of a homogenous and isotropic linearly elastic material. Let E denote the Young's modulus and A the cross-sectional area. Bars are identified by the same labels of the base joints to which they are connected. We assume that the Euler load of each bar is so large that the bars never buckle.

In the three-dimensional space of the model, two interchangeable coordinate systems are introduced. First, we consider the rectangular Cartesian coordinate system $\{O, x, y, z\}$ with the origin O at the centre

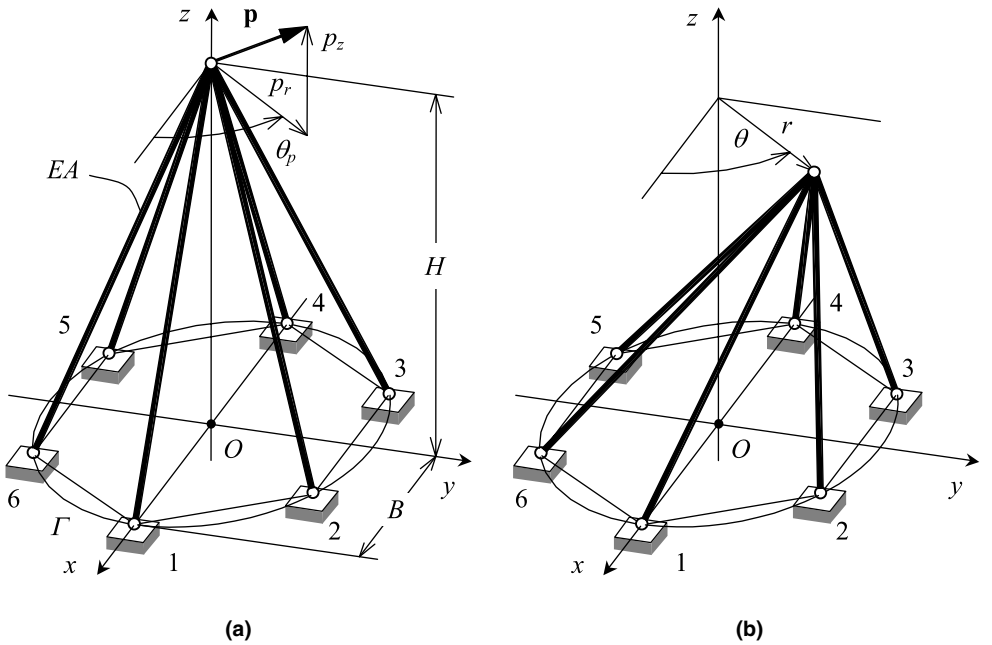

Fig. 2. The pyramidal truss: (a) reference configuration C_0, (b) current configuration C.

of the base polygon, such that the z-axis contains the height of the pyramid and the apex has a positive coordinate, and the x-axis passes through joint 1. Further, a cylindrical coordinate system $\{O, r, \theta, z\}$ is introduced according to the transformation

$$[r, \theta, z]^{\mathrm{T}} = [\sqrt{x^2 + y^2}, \arctan(y/x), z]^{\mathrm{T}}, \tag{1}$$

where $r \in [0, +\infty)$, $\theta \in [0, 2\pi)$ and $z \in (-\infty, +\infty)$. In what follows, we will call 'horizontal' those vectors (forces, displacements and so on) which are parallel to the xy-plane, and 'vertical' those parallel to the z-axis.

With the above assumptions, the position vector of the apex joint in the reference configuration C_0 is

$$\mathbf{X} = [X, Y, Z]^{\mathrm{T}} = [0, 0, H]^{\mathrm{T}}, \tag{2}$$

while the position vectors of the base joints are

$$\mathbf{X}_i = [X_i, Y_i, Z_i]^{\mathrm{T}} = [B\cos\Theta_i, B\sin\Theta_i, 0]^{\mathrm{T}}, \quad i = 1, 2, \ldots, n, \tag{3}$$

where

$$\Theta_i = 2\pi\frac{i-1}{n}, \quad i = 1, 2, \ldots, n \tag{4}$$

is the angle between the position vector $\mathbf{X}_i$ and the x-axis.

After deformation, the structure reaches a *variable configuration* C (Fig. 2b), in which the position vectors of the base joints

$$\mathbf{x}_i = \mathbf{X}_i, \quad i = 1, 2, \ldots, n \tag{5}$$

remain unchanged, while the apex joint reaches the new position

$$\mathbf{x} = [x, y, z]^{\mathrm{T}} = [r\cos\theta, r\sin\theta, z]^{\mathrm{T}} = \mathbf{X} + \mathbf{u}, \tag{6}$$

where

$$\mathbf{u} = [u, v, w]^{\mathrm{T}} = \mathbf{x} - \mathbf{X} = [r\cos\theta, r\sin\theta, z - H]^{\mathrm{T}} \tag{7}$$

is the displacement vector. Each variable configuration is determined by the knowledge of the position of the apex joint, so the coordinates r, θ and z play the role of the *Lagrangian coordinates* of the system.

As measures of deformation and stress in the bars, we adopt the *Green–Lagrange strain tensor* and the work-conjugate *second Piola–Kirchhoff stress tensor,* respectively. Thus, the axial components of strain are

$$\varepsilon_i = \frac{l_i^2 - L^2}{2L^2}, \quad i = 1, 2, \ldots, n, \tag{8}$$

where

$$l_i^2 = (\mathbf{x} - \mathbf{x}_i)^{\mathrm{T}}(\mathbf{x} - \mathbf{x}_i) = r^2 - 2rB\cos(\theta - \theta_i) + B^2 + z^2, \quad i = 1, 2, \ldots, n \tag{9}$$

are the squares of the bar lengths in the configuration C, while the axial components of stress are

$$\sigma_i = E\varepsilon_i, \quad i = 1, 2, \ldots, n. \tag{10}$$

The *strain energy of the system*, W, is the sum of the contributions

$$W_i = \frac{1}{2}EAL\varepsilon_i^2, \quad i = 1, 2, \ldots, n \tag{11}$$

relative to the n bars. By substituting (8) and (9) in (11), and carrying out the summation, we obtain

$$W(r,\theta,z)=\sum_{i=1}^{n}W_i=\frac{1}{2}EAL\sum_{i=1}^{n}\varepsilon_i^2=\frac{nEA}{8L^3}[(r^2+z^2-H^2)^2+2B^2r^2]=W(r,z), \tag{12}$$

which, rather unexpectedly, turns out to be a function of the r and z coordinates only. As a consequence, the geometric n-fold rotational symmetry of the initial configuration turns into an axial symmetry for the structural problem. Thus, apart from possible asymmetries introduced by a non-axisymmetric applied load, we expect the elastic response of the system to be independent of the coordinate θ.

As the load

$$\lambda\mathbf{p}=\lambda[p_x,p_y,p_z]^{\mathrm{T}}=\lambda[p_r\cos\theta_p,p_r\sin\theta_p,p_z]^{\mathrm{T}} \tag{13}$$

does not depend upon C, it is conservative, so we can define the *load potential energy*

$$V(\lambda;r,\theta,z)=-\lambda\mathbf{p}^{\mathrm{T}}\mathbf{u}=-\lambda(p_xr\cos\theta+p_yr\sin\theta+p_zz)+\lambda p_zH. \tag{14}$$

By summing the contributions (12) and (14), we obtain the *total potential energy* of the system

$$\Pi(\lambda;r,\theta,z)=W(r,z)+V(\lambda;r,\theta,z). \tag{15}$$

The stationary conditions for Π with respect to the Lagrangian coordinates,

$$\begin{cases} f_r=\dfrac{\partial\Pi}{\partial r}=\dfrac{nEA}{2L^3}r(r^2+z^2-H^2+B^2)-\lambda p_r\cos(\theta-\theta_p)=0,\\ f_\theta=\dfrac{1}{r}\dfrac{\partial\Pi}{\partial\theta}=\lambda p_r\sin(\theta-\theta_p)=0,\\ f_z=\dfrac{\partial\Pi}{\partial z}=\dfrac{nEA}{2L^3}z(r^2+z^2-H^2)-\lambda p_z=0 \end{cases} \tag{16}$$

constitute the governing set of non-linear equations whose solutions are the equilibrium configurations of the system for variable λ. In the four-dimensional space spanned by λ and by the Lagrangian coordinates, r, θ, and z, the solutions of (16) constitute a set of points, referred to as the *equilibrium path* of the system. The geometrical properties of the path are strictly related to the mechanical response of the structure under the assigned load condition (see, in particular, Sewell, 1966; Wempner, 1971).

3. Stability analysis

3.1. Neutral equilibrium surfaces

Before going to present the solutions of (16), we want to discuss the conditions for which the equilibrium state of the system in the configuration C is stable. To this aim, the *Hessian matrix* $\mathbf{K}$ of Π needs to be evaluated in the considered configuration. As is well known, the equilibrium is stable if $\mathbf{K}$ is positive definite, neutrally stable if $\mathbf{K}$ is positive semi-definite, and unstable if $\mathbf{K}$ is indefinite. In the first case, all eigenvalues of the Hessian matrix are positive; in the second case, only one eigenvalue is zero while the remaining are positive; finally, in the third case, at least one eigenvalue is negative.

On the equilibrium paths, configurations of neutrally stable equilibrium correspond to *critical points*, which in turn may be either *limit points*, where the load parameter λ is stationary, or *bifurcation points*, where the tangent to the path is no longer unique due to the presence of one or more intersecting secondary branches (single or multiple bifurcation) (see, for instance, Sewell, 1968; Thompson and Hunt, 1984). Since the mechanical behaviour of the system differs greatly in each of the aforementioned situations, a deeper

investigation about the nature of the criticality is essential. This task requires the eigenvectors of **K** to be determined as well.

By further differentiation of (16) we obtain

$$\mathbf{K} = \begin{bmatrix} f_{rr} & f_{r\theta} & f_{rz} \\ f_{\theta r} & f_{\theta\theta} & f_{\theta z} \\ f_{zr} & f_{z\theta} & f_{zz} \end{bmatrix} = \frac{nEA}{2L^3} \begin{bmatrix} 3r^2 + z^2 - H^2 + B^2 & 0 & 2rz \\ 0 & r^2 + z^2 - H^2 + B^2 & 0 \\ 2rz & 0 & r^2 + 3z^2 - H^2 \end{bmatrix}. \tag{17}$$

The load potential energy V is linear with respect to the displacement **u**, so the Hessian matrix does not depend on the applied load; consequently, if any region exists in the coordinate space associated to stable equilibrium states, this will be independent of the load. From (17) we see that **K** does not depend on the coordinate θ, so the regions of stable equilibrium are axisymmetric about the z-axis; moreover, since the substitution of $+z$ with $-z$ does not alter the sign of (17), the stability regions are symmetric with respect to the xy-plane as well.

By solving the characteristic equation, $\det(\mathbf{K} - \omega\mathbf{I}) = 0$, where **I** is the identity matrix, the *eigenvalues* of **K** are determined as

$$\omega_1 = \frac{nEA}{2L^3}\left[2r^2 + 2z^2 - H^2 + \frac{B^2}{2} - \sqrt{\left(r^2 - z^2 + \frac{B^2}{2}\right)^2 + 4r^2z^2}\right], \tag{18a}$$

$$\omega_2 = \frac{nEA}{2L^3}(r^2 + z^2 - H^2 + B^2), \tag{18b}$$

$$\omega_3 = \frac{nEA}{2L^3}\left[2r^2 + 2z^2 - H^2 + \frac{B^2}{2} + \sqrt{\left(r^2 - z^2 + \frac{B^2}{2}\right)^2 + 4r^2z^2}\right]. \tag{18c}$$

By setting $\omega_1 = 0$ in (18a), $\omega_2 = 0$ in (18b) and $\omega_3 = 0$ in (18c), respectively, we obtain the equations:

$$(\Omega_1) \quad z = \pm z_1(r) = \pm\sqrt{\frac{2H^2}{3} - \frac{B^2}{2} - r^2 + \sqrt{\left(\frac{H^2}{3} - \frac{B^2}{2}\right)^2 + \frac{2B^2r^2}{3}}}, \tag{19a}$$

$$(\Omega_2) \quad z = \pm z_2(r) = \pm\sqrt{H^2 - B^2 - r^2}, \tag{19b}$$

$$(\Omega_3) \quad z = \pm z_3(r) = \pm\sqrt{\frac{2H^2}{3} - \frac{B^2}{2} - r^2 - \sqrt{\left(\frac{H^2}{3} - \frac{B^2}{2}\right)^2 + \frac{2B^2r^2}{3}}}, \tag{19c}$$

which in the xyz-space represent three closed surfaces. As expected, these are surfaces of revolution about the z-axis and symmetrical with respect to the xy-plane. The configurations where the apex joint of the pyramid lies upon one of the above surfaces are of neutrally stable equilibrium; therefore, we will term Ω_1, Ω_2 and Ω_3 the *neutral equilibrium surfaces*. In passing, we note how the above surfaces depend uniquely upon the characteristic lengths of the model.

The surface Ω_1 separates the xyz-space into two parts. The inner part, denoted by Ω_1^-, contains the origin O and represents the set of points where the eigenvalue ω_1 assumes negative values, while the outer complementary part, denoted by Ω_1^+, is the locus of points where ω_1 is strictly positive. By setting $z = 0$ in (19a) and solving for r, we obtain the value of the *equatorial radius* of Ω_1, $R_1 = H$; conversely, by putting $r = 0$ in (19a) and solving for z, we find the distance $Z_1 = z_1(0)$ between the origin O and the *poles*, P_1^+ and P_1^-, where the surface Ω_1 intersects the positive and negative sides of the z-axis, respectively:

$$Z_1 = z_1(0) = \begin{cases} H/\sqrt{3} & \text{if } H < H_0, \\ \sqrt{H^2 - B^2} & \text{if } H \geqslant H_0. \end{cases} \tag{20}$$

In (20), $H_0 = \sqrt{3/2}B$ is a particular value of the height of the truss, whose physical meaning will soon become evident. In both cases given by (20), $R_1 > Z_1$, so the surface Ω_1 appears to be 'squeezed' along the axis of revolution, like an oblate spheroid.

The surfaces Ω_2 and Ω_3 are real if and only if $H \geqslant B$, but for $H = B$ both the surfaces shrink to the origin O. The surface Ω_2 is manifestly the sphere with centre at the origin O and radius $R_2 = \sqrt{H^2 - B^2} < R_1$, so that the distance between its poles, P_2^+ and P_2^-, and the origin is simply

$$Z_2 = z_2(0) = R_2. \tag{21}$$

The equatorial radius of Ω_3 is $R_3 = \sqrt{(H^2 - B^2)/3} = R_2/\sqrt{3} < R_2 < R_1$, while the distance between its poles, P_3^+ and P_3^-, and the origin is

$$Z_3 = z_3(0) = \begin{cases} \sqrt{H^2 - B^2} & \text{if } H < H_0, \\ H/\sqrt{3} & \text{if } H \geqslant H_0. \end{cases} \tag{22}$$

In both cases of (22), $R_3 < Z_3$, so the surface Ω_3 appears to be 'pulled' along its axis of revolution, like a prolate spheroid. As before, we indicate with Ω_2^- and Ω_3^-, respectively, the regions of the coordinate space where the eigenvalues ω_2 and ω_3 assume negative values, and with Ω_2^+ and Ω_3^+ their complementary parts.

Fig. 3a and b show the meridians of the neutral equilibrium surfaces in the rz-plane for the values $B = 100$ cm, $H_0 = \sqrt{3/2}B \approx 122.474$ cm and two different values of the height H.

By keeping B fixed and changing H, the neutral equilibrium surfaces Ω_1 and Ω_3 assume a continuous sequence of different shapes, which in the extreme cases are very similar to an apple-shaped ellipsoid and to a spindle-shaped ellipsoid, respectively. Fig. 4a–d show a cutaway view of the neutral equilibrium surfaces for increasing values of H.

It is quite simple to verify that $\Omega_3^- \subseteq \Omega_2^-$. More precisely, if $H < H_0$ the surface Ω_3 is internally tangent to the sphere Ω_2 at the poles ($P_2^+ \equiv P_3^+$ and $P_2^- \equiv P_3^-$), while if $H > H_0$ the two surfaces have no common points. In the first case, two eigenvalues vanish simultaneously at the points of tangency; these will correspond to two *double critical points*. Likewise, we may verify that $\Omega_2^- \subseteq \Omega_1^-$. In particular, if $H < H_0$ the sphere Ω_2 is entirely enclosed within the region Ω_1^-, while if $H > H_0$ the sphere Ω_2 is internally tangent to surface Ω_3 at the poles ($P_1^+ \equiv P_2^+$ and $P_1^- \equiv P_2^-$); these, due to the simultaneous vanishing of two eigenvalues, will be related to two double critical points. When the height of the pyramid is $H = H_0$, the three surfaces of neutral equilibrium, Ω_1, Ω_2 and Ω_3, are tangent to each other at their poles ($P_1^+ \equiv P_2^+ \equiv P_3^+$ and $P_1^- \equiv P_2^- \equiv P_3^-$), where they possess a common horizontal tangent plane; since here three eigenvalues vanish simultaneously, the points of tangency will correspond to two *triple critical points*. All in all, based upon the last observations, H_0 can be quite rightly defined the *critical height* of the pyramid.

In conclusion, the region of the xyz-space where all the eigenvalues assume positive values, Ω_1^+, is the *stability region*, where equilibrium of the system is always stable. The points where the equilibrium path will intersect the surface Ω_1 will correspond to the first critical load, while the intersections of the path with the surfaces Ω_2 and Ω_3 will correspond to critical points of higher order. Consequently, ω_1 is the minimum eigenvalue which need to be monitored to prevent any possible instability phenomenon.

3.2. Eigenvectors corresponding to zero eigenvalues

In order to establish a distinction between bifurcation and limit points, the eigenvectors corresponding to zero eigenvalues need to be determined. The eigenvector $\mathbf{a}_k = [a_{kr}, a_{k\theta}, a_{kz}]^{\mathrm{T}}$ paired to the eigenvalue ω_k, given by each of (18a,b,c), for $k = 1, 2, 3$, is obtained by solving the set of linear equations

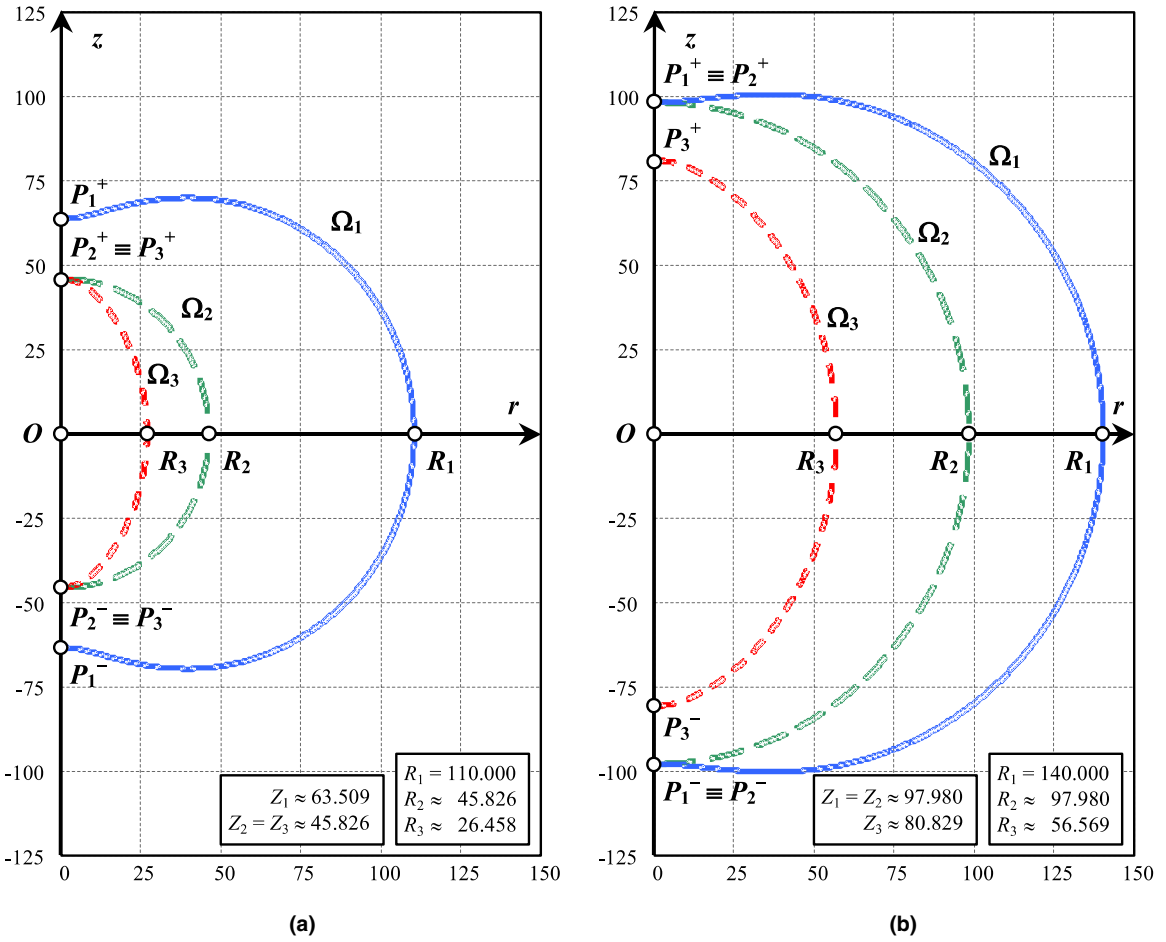

Fig. 3. The meridians of the neutral equilibrium surfaces: (a) $H = 110$ cm $< H_0$, (b) $H = 140$ cm $> H_0$.

$$(\mathbf{K} - \omega_k \mathbf{I})\mathbf{a}_k = \mathbf{0} \tag{23}$$

together with the normality condition

$$a_{kr}^2 + a_{k\theta}^2 + a_{kz}^2 = 1. \tag{24}$$

If $\omega_k = 0$, the equation set (23) becomes

$$\begin{cases} [3r^2 + z_k^2(r) - H^2 + B^2]a_{kr} + 2rz_k(r)a_{kz} = 0, \\ [r^2 + z_k^2(r) - H^2 + B^2]a_{k\theta} = 0, \\ 2rz_k(r)a_{kr} + [r^2 + 3z_k^2(r) - H^2]a_{kz} = 0, \end{cases} \tag{25}$$

where $z_k(r)$ is given by (19a) or (19b) or, finally, (19c). Thus, the three eigenvectors result

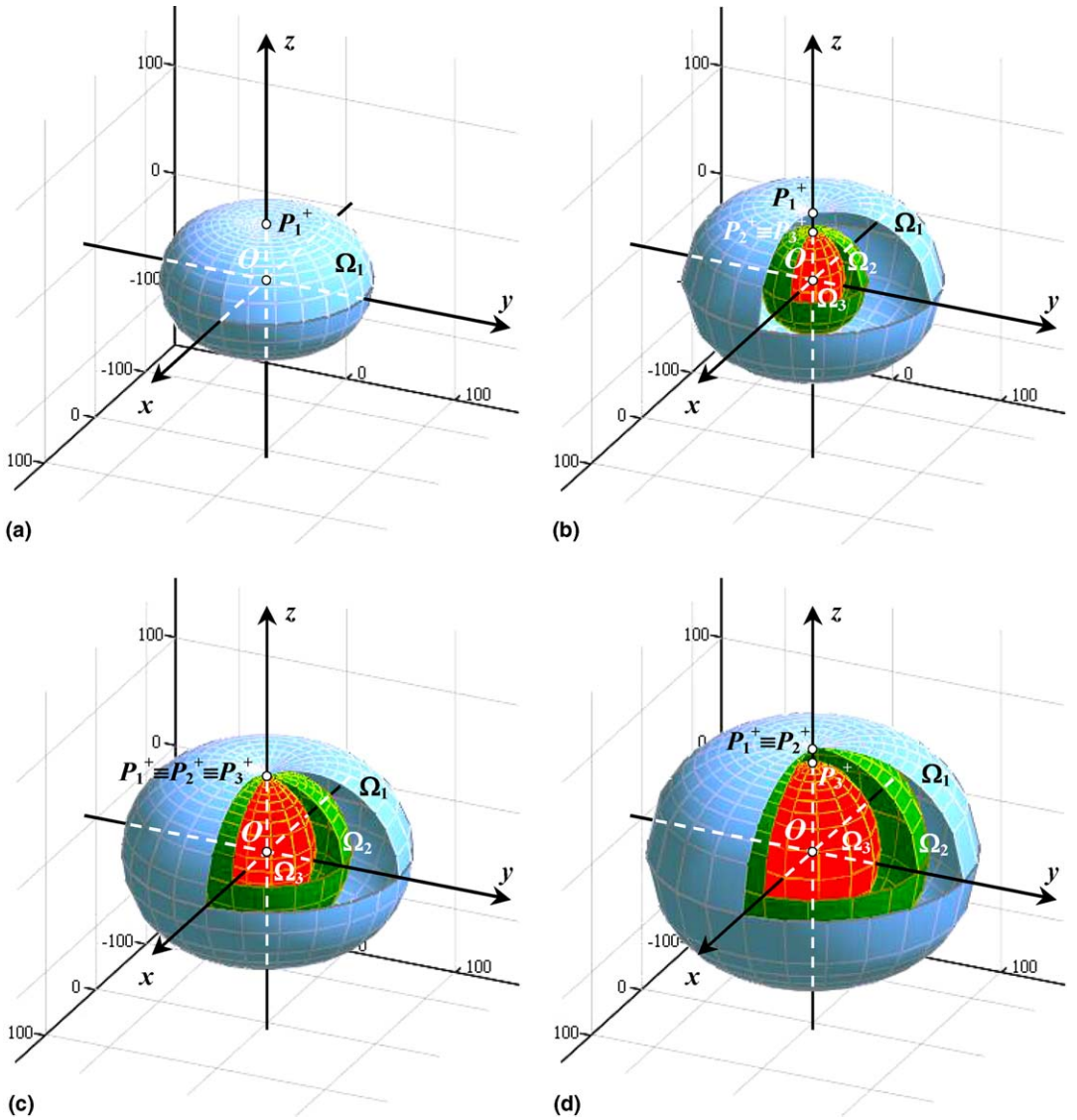

Fig. 4. The neutral equilibrium surfaces: (a) $H = 90\ \text{cm} < B = 100\ \text{cm}$, (b) $B < H = 100\ \text{cm} < H_0$, (c) $H = H_0 \approx 122.474\ \text{cm}$, (d) $H = 140\ \text{cm} > H_0$.

$$(\mathbf{a}_1)\quad \begin{cases} a_{1r} = -\dfrac{r^2 + 3z_1^2(r) - H^2}{2rz_1(r)}\, a_{1z}, \\ a_{1\theta} = 0, \\ a_{1z} = \dfrac{1}{\sqrt{1 + \left[\dfrac{r^2 + 3z_1^2(r) - H^2}{2rz_1(r)}\right]^2}}, \end{cases} \tag{26a}$$

$$(\mathbf{a}_2)\quad \begin{cases} a_{2r} = 0, \\ a_{2\theta} = 1, \\ a_{2z} = 0, \end{cases} \tag{26b}$$

$$(\mathbf{a}_3)\quad \begin{cases} a_{3r} = -\dfrac{r^2 + 3z_3^2(r) - H^2}{2rz_3(r)} a_{3z}, \\ a_{3\theta} = 0, \\ a_{3z} = \dfrac{1}{\sqrt{1 + \left[\dfrac{r^2 + 3z_3^2(r) - H^2}{2rz_3(r)}\right]^2}}. \end{cases} \tag{26c}$$

In the xyz-space, $\mathbf{a}_2$ is a unit vector acting in the circumferential direction, that is, $\mathbf{a}_2$ is always tangent to the parallels of the sphere Ω_2. On the contrary, $\mathbf{a}_1$ and $\mathbf{a}_3$ are unit vectors lying on the planes $\theta = \text{const}$. The components of $\mathbf{a}_1$ and $\mathbf{a}_3$ are functions of the radius r alone. If $r = 0$, the expressions (26a) and (26c) are not defined. In these cases, carrying out the limits for $r \to 0$, we obtain

$$\begin{cases} a_{1r}|_{r=0} = 0, \\ a_{1\theta}|_{r=0} = 0, \ \text{if } H < H_0, \\ a_{1z}|_{r=0} = 1, \end{cases} \quad \text{or} \quad \begin{cases} a_{1r}|_{r=0} = -1, \\ a_{1\theta}|_{r=0} = 0, \ \text{if } H > H_0, \\ a_{1z}|_{r=0} = 0, \end{cases} \tag{27a, b}$$

and

$$\begin{cases} a_{3r}|_{r=0} = 1, \\ a_{3\theta}|_{r=0} = 0, \ \text{if } H < H_0, \\ a_{3z}|_{r=0} = 0, \end{cases} \quad \text{or} \quad \begin{cases} a_{3r}|_{r=0} = 0, \\ a_{3\theta}|_{r=0} = 0, \ \text{if } H > H_0. \\ a_{3z}|_{r=0} = 1. \end{cases} \tag{28a, b}$$

In the intermediate case, $H = H_0$, the three eigenvalues vanish simultaneously at $r = 0$, so that any triplet of mutually orthogonal unit vectors may be assumed as the eigenvectors.

Eqs. (26a) and (26c) are also undefined for $r = R_1$ and $r = R_3$, respectively. Carrying out the limits for $r \to R_1$ and $r \to R_3$, we find the expressions

$$\begin{cases} a_{1r}|_{r=R_1} = 0, \\ a_{1\theta}|_{r=R_1} = 0, \\ a_{1z}|_{r=R_1} = 1, \end{cases} \quad \text{and} \quad \begin{cases} a_{3r}|_{r=R_3} = 1, \\ a_{3\theta}|_{r=R_3} = 0, \\ a_{3z}|_{r=R_3} = 0. \end{cases} \tag{29a, b}$$

Fig. 5 shows a plot of the eigenvectors $\mathbf{a}_1$ and $\mathbf{a}_3$ in the rz-plane, together with the meridians of the corresponding neutral equilibrium surfaces. The remaining eigenvector $\mathbf{a}_2$ is not shown because it is perpendicular to the representation plane. The same numerical values of the previous figures were used.

3.3. Scalar products and post-critical behaviour

When a single eigenvalue, say ω_k, vanishes, then a *distinct critical point* has been reached along the equilibrium path (Thompson and Hunt, 1984; Kouhia and Mikkola, 1989); however, in order to decide what kind of instability will actually take place, the scalar product $V_k = \mathbf{p}^{\mathrm{T}}\mathbf{a}_k$, between the reference load vector $\mathbf{p}$ and the corresponding eigenvector $\mathbf{a}_k$, needs to be evaluated. In fact, if $V_k \neq 0$, the load parameter λ is locally stationary: the critical point is a limit point and loss of stability occurs by snap-through. Instead, if $V_k = 0$, the tangent to the path is no longer unique: the critical point is a bifurcation point and instability manifests itself as buckling.

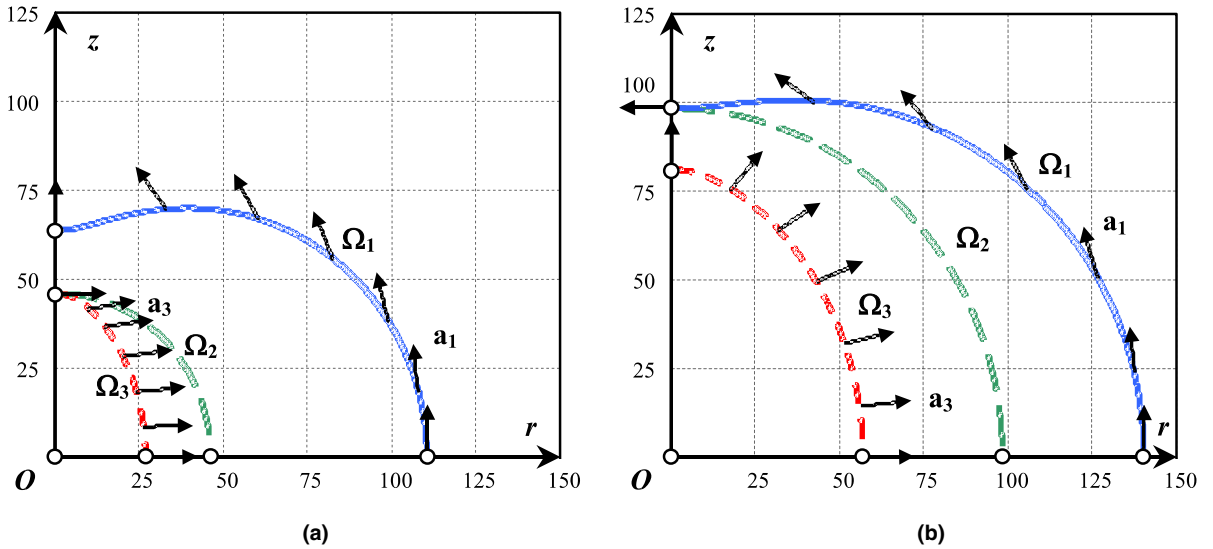

Fig. 5. Eigenvectors corresponding to zero eigenvalues: (a) $H = 110$ cm $< H_0$, (b) $H = 140$ cm $< H_0$.

For the structural problem under consideration, the scalar products relative to the three eigenvalues result

$$V_1 = \mathbf{p}^{\mathrm{T}}\mathbf{a}_1 = p_r a_{1r}\cos(\theta - \theta_p) + p_z a_{1z}, \tag{30a}$$

$$V_2 = \mathbf{p}^{\mathrm{T}}\mathbf{a}_2 = -p_r \sin(\theta - \theta_p), \tag{30b}$$

$$V_3 = \mathbf{p}^{\mathrm{T}}\mathbf{a}_3 = p_r a_{3r}\cos(\theta - \theta_p) + p_z a_{3z}. \tag{30c}$$

In particular, since ω_1 is the minimum eigenvalue, the first scalar product (30a) is the one to be evaluated to decide what kind of instability is associated to the first critical load. More generally, as previously noticed, there are some points of the xyz-space where two or three eigenvalues may vanish simultaneously. These correspond to *compound critical points* (Kouhia and Mikkola, 1999). The post-critical behaviour of the structure in these points becomes more involved: both forms of instability may coexist and interact. Accordingly, all the above scalar products need to be considered.

4. Self-equilibrated load-free configurations

In this brief section, we search for those configurations of the pyramidal truss where an equilibrium state may take place in absence of applied loads, irrespective of the state of stress in the bars. The knowledge of these configurations is of great importance in stability analysis, since they constitute points of obligatory passage for the equilibrium paths. In the coordinate space, these load-free equilibrium configurations may correspond either to isolated points or even to curves, the latter representing finite mechanisms (Kumar and Pellegrino, 2000; Tarnai, 2003).

By putting $\lambda = 0$ in (15), the total potential energy Π of the system reduces to the strain energy function W; therefore, to decide about the quality of the equilibrium, namely stable or not, it is sufficient again to examine the sign of the Hessian matrix $\mathbf{K}$ of Π, here still given by (17), and the sign of its eigenvalues.

The load-free configurations can immediately be determined by solving the equation set (16), where we let $\lambda = 0$. Thus, we find four solutions:

$$\begin{cases} r = 0, \\ z = H, \end{cases} \quad \begin{cases} r = 0, \\ z = -H, \end{cases} \tag{31a, b}$$

$$\begin{cases} r = 0, \\ z = 0, \end{cases} \quad \begin{cases} r = \sqrt{H^2 - B^2} = R_2, \\ z = 0 \end{cases} \tag{31c, d}$$

whose mechanical meaning is made clear by recalling the definition of the neutral equilibrium surfaces.

In the xyz-space, these solutions represent three isolated points and a closed curve (Fig. 6). In particular, solutions (31a) and (31b) correspond to the reference configuration, C_0, and to its symmetric, $-C_0$, relative to the xy-plane, respectively. Both points belong to the stability region Ω_1^+. At these configurations, the total potential energy Π attains a local minimum, so the equilibrium is stable, but, since $W = 0$, the bars are stress-free. Solution (31c) represents the origin O of the coordinate system, which belongs to the region Ω_3^-. At O, Π attains a local maximum, so the equilibrium is unstable, but, since $W > 0$, now the bars are stressed. Finally, solution (31d) represents the circle Γ_2 of the xy-plane with its centre at O and radius R_2, namely the equatorial circle of the neutral equilibrium surface Ω_2; this circle is composed of real points if and only if $H \geqslant B$. All points of this circle are saddle points for Π; moreover, since $W > 0$, the bars are stressed. These configurations are no doubt globally unstable, but, at a deeper investigation, one can easily verify that, if each degree of freedom could be activated individually, then the equilibrium would be stable with respect to the r-coordinate, unstable with respect to z, and neutral with respect to θ. Finally, it is an easy task to recognise how these load-free equilibrium configurations correspond to cases where the pyramid as a whole is flattened in the xy-plane, while the apex joint runs along Γ_2 in the absence of external loads.

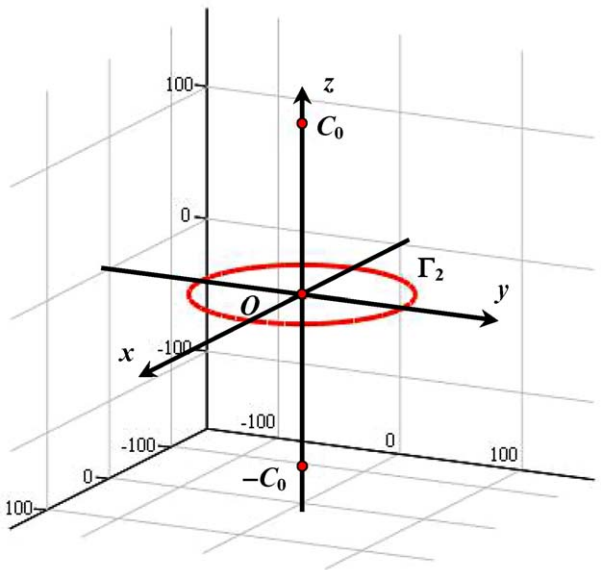

Fig. 6. Self-equilibrated load-free configurations.

5. Equilibrium paths

In this section, we solve the set of the equilibrium equations (16) for three relevant loading conditions. To better understand the mechanical behaviour of the structure in each case, we give a graphical representation of the obtained solutions. Strictly speaking, the equilibrium paths should be plotted in the four-dimensional space spanned by the load multiplier, λ, and the Lagrangian coordinates, r, θ, and z. However, we consider appropriate to give also the plots of the paths in the three-dimensional space of x, y, z, where the curves are immediately identified with the trajectories of the apex joint. For a better understanding, the pyramidal truss in its reference configuration will be reproduced in the following figures as well.

5.1. Vertical load

The first load condition is characterised by

$$p_r = 0 \quad \text{and} \quad p_z \neq 0. \tag{32a, b}$$

Since the load does not break the rotational symmetry of the system, we expect the solution to be independent of the angle θ. Actually, the second equation of (16) turns out to be identically satisfied, while θ disappears from the remaining equations. The solution of the equilibrium equations consists of the two following groups of expressions

$$\begin{cases} \lambda = \dfrac{1}{2}\dfrac{1}{p_z}\dfrac{nEA}{L^3} z(z^2 - H^2), \\ r = 0, \\ \theta = \text{undef.}, \\ z \in (-\infty, +\infty), \end{cases} \quad \text{or} \quad \begin{cases} \lambda = -\dfrac{1}{2}\dfrac{1}{p_z}\dfrac{nEA}{L^3} B^2 z, \\ r = \sqrt{H^2 - B^2 - z^2}, \\ \theta \in [0, 2\pi), \\ z \in [-\sqrt{H^2 - B^2}, \sqrt{H^2 - B^2}]. \end{cases} \tag{33a, b}$$

Eq. (33a) define the *primary branch* of the path, which in the xyz-space is plotted as a straight line coincident with the z-axis. Eq. (33b) represent a sphere perfectly fitting in the neutral equilibrium surface Ω_2. Any curve of this sphere is a feasible sequence of equilibrated configurations. However, considering the direction of the applied load, we may distinguish, for each value of θ, a *secondary branch* coincident with a meridian and, for each value of z, a *tertiary branch* represented by a parallel. Therefore, the surface Ω_2 contains an infinite number of secondary branches (the meridians), and an infinite number of tertiary branches (the parallels).

In Fig. 7 several projections and views of the equilibrium path are given for the following numerical values: $n = 6$, $B = 100$ cm, $H = 130$ cm, $EA = 20000$ N, $p_z = -100$ N. The continuous curve represents the primary branch, while the dashed curve is the secondary one. We also notice that the surface (33b), which is a sphere in the xyz-space (Fig. 7a–c), appears as an ellipse when plotted in the $rz\lambda$-space (Fig. 7d–f).

Provided that $H \geqslant B$, the primary branch intersects the three neutral equilibrium surfaces at their poles. Since four of these points are in pairs coincident, we obtain four critical points in all, that is two simple limit points, L_1 and L_2:

$$\begin{cases} \lambda = -\dfrac{1}{3\sqrt{3}}\dfrac{1}{p_z}\dfrac{nEA}{L^3} H^3, \\ r = 0, \\ \theta = \text{undef.}, \\ z = \dfrac{H}{\sqrt{3}}, \end{cases} \quad \begin{cases} \lambda = \dfrac{1}{3\sqrt{3}}\dfrac{1}{p_z}\dfrac{nEA}{L^3} H^3, \\ r = 0, \\ \theta = \text{undef.}, \\ z = -\dfrac{H}{\sqrt{3}} \end{cases} \tag{34a, b}$$

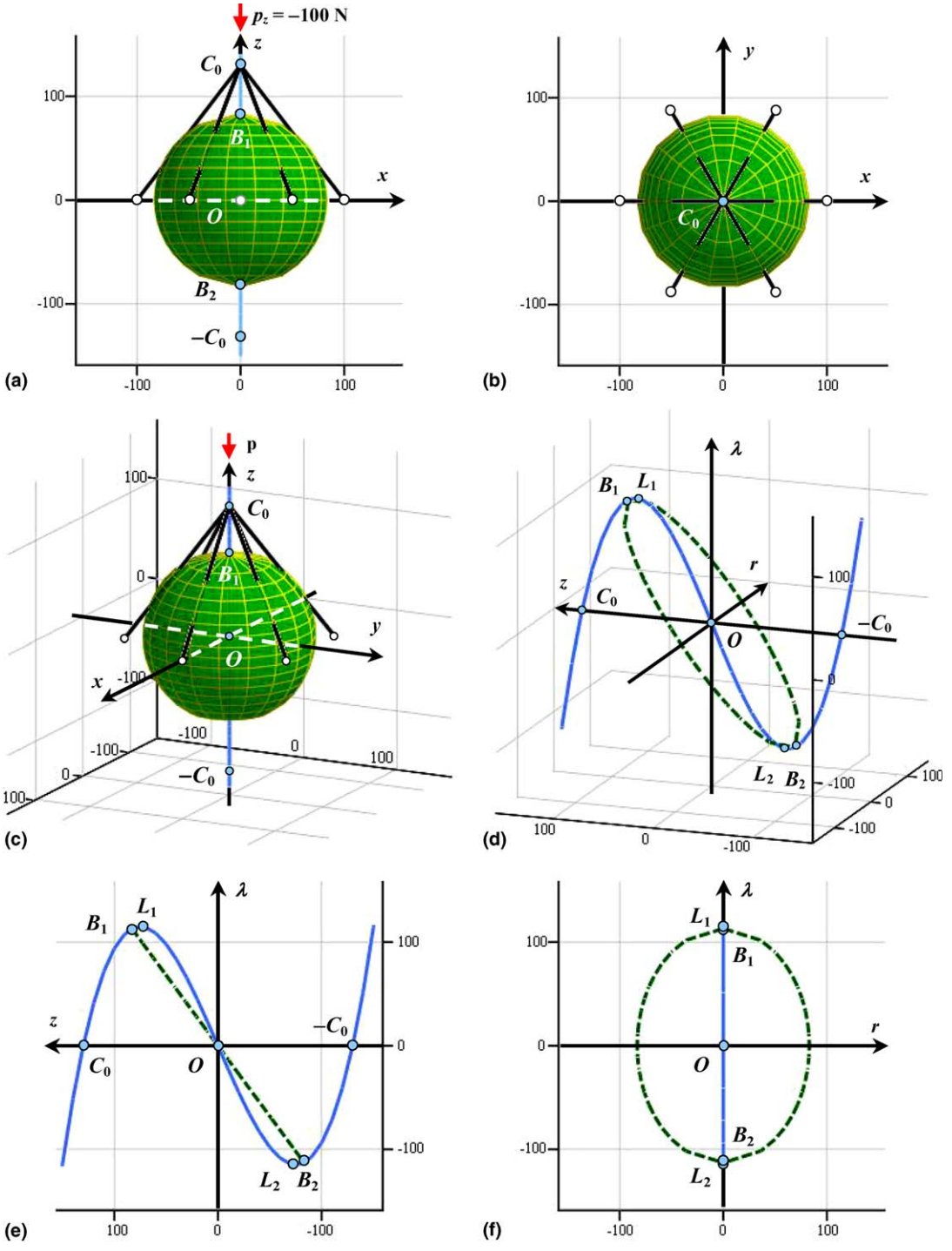

Fig. 7. Equilibrium path of the pyramidal truss subjected to a vertical load: (a) projection on the xz-plane, (b) projection on the xy-plane, (c) view in the xyz-space, (d) view in the $rz\lambda$-space, (e) projection on the $z\lambda$-plane, (f) projection on the $r\lambda$-plane.

and two double bifurcation points, B_1 and B_2:

$$\begin{cases} \lambda = -\dfrac{1}{2}\dfrac{1}{p_z}\dfrac{nEA}{L^3}B^2\sqrt{H^2-B^2}, \\ r = 0, \\ \theta = \text{undef.}, \\ z = \sqrt{H^2-B^2}, \end{cases} \quad \begin{cases} \lambda = \dfrac{1}{2}\dfrac{1}{p_z}\dfrac{nEA}{L^3}B^2\sqrt{H^2-B^2}, \\ r = 0, \\ \theta = \text{undef.}, \\ z = -\sqrt{H^2-B^2}. \end{cases} \tag{35a, b}$$

When the primary branch is travelled starting from the reference configuration, C_0, the limit point precedes the bifurcation if $H < H_0$, while it follows if $H > H_0$. If $H = H_0$, these critical points coincide at a *triple critical point*, namely we obtain a *hill-top multiple branching point* (Thompson and Hunt, 1984). Finally, we observe the interesting feature that the positions in xyz-space of the above critical points depend only on the values of the characteristic lengths B and H, neither on the load nor on the elastic properties of the bars.

Most numerical path-tracing procedures would encounter serious difficulties in finding the tangent vectors to the secondary branches at the bifurcation points, as well as in attempting to trace any curve lying on the sphere, which is made up completely of bifurcation points.

5.2. Horizontal load

The second loading condition is characterised by

$$p_r \neq 0 \quad \text{and} \quad p_z = 0. \tag{36a, b}$$

Now the applied load breaks the rotational symmetry of the system, so the solution is expected to depend on the angle θ. Actually, the complete solution of the equilibrium equation (16) is given by the following four groups of expressions

$$\begin{cases} \lambda = \dfrac{1}{2}\dfrac{1}{p_r}\dfrac{nEA}{L^3}B^2\sqrt{H^2-z^2}, \\ r = \sqrt{H^2-z^2}, \\ \theta = \theta_p, \\ z \in [-H, H], \end{cases} \text{ or } \begin{cases} \lambda = -\dfrac{1}{2}\dfrac{1}{p_r}\dfrac{nEA}{L^3}B^2\sqrt{H^2-z^2}, \\ r = \sqrt{H^2-z^2}, \\ \theta = \theta_p + \pi, \\ z \in [-H, H], \end{cases} \text{ or } \tag{37a, b}$$

$$\begin{cases} \lambda = \dfrac{1}{2}\dfrac{1}{p_r}\dfrac{nEA}{L^3}r(r^2-H^2+B^2), \\ r \in [0, +\infty), \\ \theta = \theta_p, \\ z = 0 \end{cases} \text{ or } \begin{cases} \lambda = -\dfrac{1}{2}\dfrac{1}{p_r}\dfrac{nEA}{L^3}r(r^2-H^2+B^2), \\ r \in [0, +\infty), \\ \theta = \theta_p + \pi, \\ z = 0, \end{cases} \tag{37c, d}$$

In xyz-space, the four parts of the solution (37) lie in the vertical plane containing the z-axis and the direction of the reference load vector. In particular, (37a,b) represent a circle with its centre at the origin O and radius H, which constitutes the *primary branch* of the equilibrium path; instead, (37c,d) represent a straight line of the xy-plane, which constitutes the *secondary branch*. Both branches are always present, regardless of the height of the truss. In addition, if $H \geqslant B$, a *tertiary branch*, represented by the circle Γ_2, given by (31d), completes the equilibrium path; the remaining load-free equilibrium configurations (31a,b,c) are already included in solution (37). Fig. 8 shows several projections and views of the equilibrium path obtained for the same numerical values considered before, except for the load which is now $p_r = 150$ N, with $\theta_p = 75°$. Again, the continuous curve represents the primary branch, the dashed curve is the secondary one, and the dotted curve is the tertiary branch.

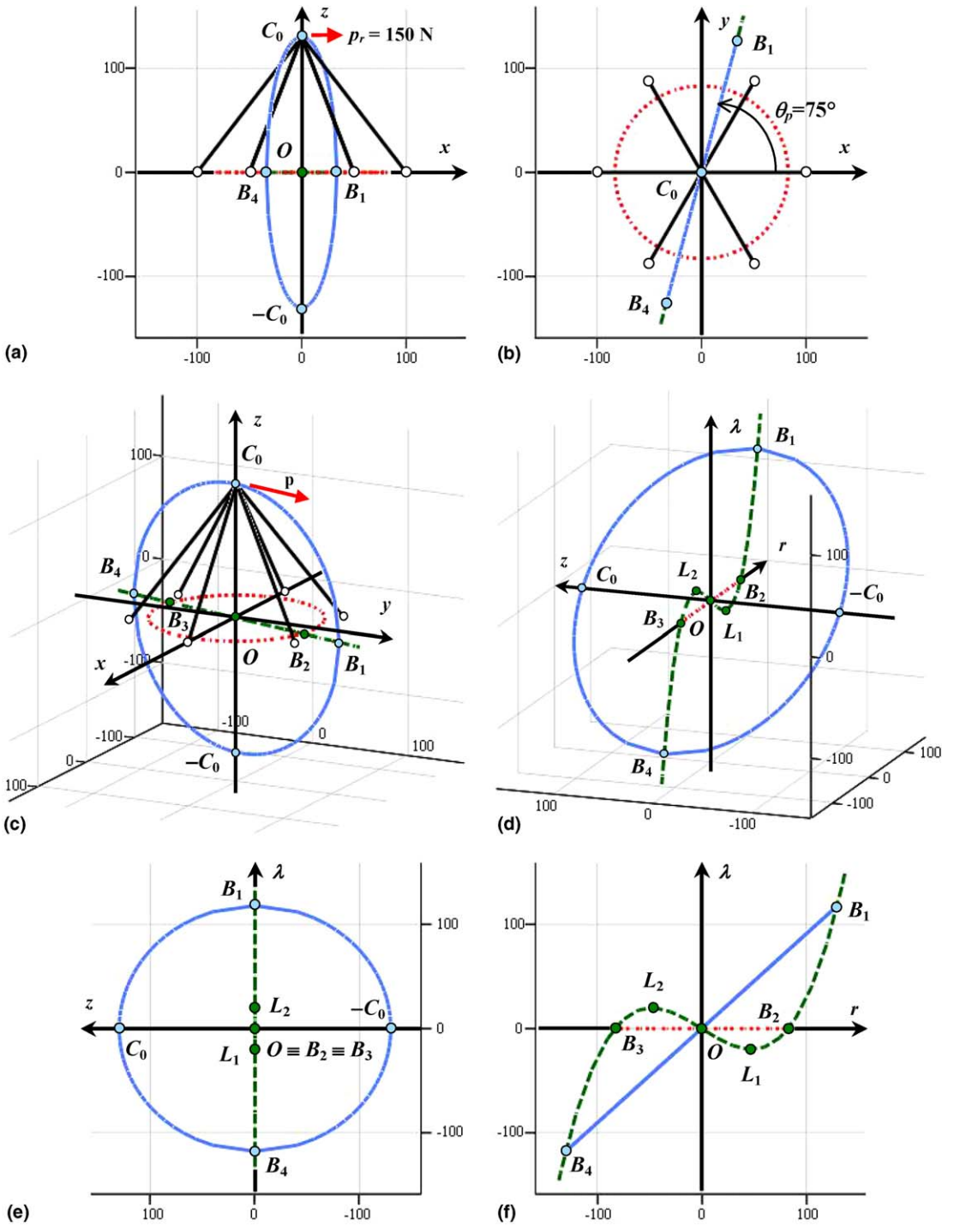

Fig. 8. Equilibrium path of the pyramidal truss subjected to a horizontal load: (a) projection on the xz-plane, (b) projection on the xy-plane, (c) view in the xyz-space, (d) view in the $rz\lambda$-space, (e) projection on the $z\lambda$-plane, (f) projection on the $r\lambda$-plane.

Critical points are detected at the intersections between the path and the neutral equilibrium surfaces. In particular, the primary branch intersects the surface Ω_1, at two bifurcation points, B_1 and B_4:

$$\begin{cases} \lambda = \dfrac{1}{2}\dfrac{1}{p_r}\dfrac{nEA}{L^3}B^2H, \\ r = H, \\ \theta = \theta_p, \\ z = 0, \end{cases} \qquad \begin{cases} \lambda = -\dfrac{1}{2}\dfrac{1}{p_r}\dfrac{nEA}{L^3}B^2H, \\ r = H, \\ \theta = \theta_p + \pi, \\ z = 0, \end{cases} \tag{38a, b}$$

where it meets the secondary branch; moreover, if $H \geqslant B$, the secondary branch also intersects the surface Ω_2 at two further bifurcation points, B_2 and B_3:

$$\begin{cases} \lambda = 0, \\ r = \sqrt{H^2 - B^2}, \\ \theta = \theta_p, \\ z = 0, \end{cases} \qquad \begin{cases} \lambda = 0, \\ r = \sqrt{H^2 - B^2}, \\ \theta = \theta_p + \pi, \\ z = 0, \end{cases} \tag{39a, b}$$

where it meets the tertiary branch; finally, the secondary branch intersects the surface Ω_3 at two limit points, L_1 and L_2:

$$\begin{cases} \lambda = -\dfrac{1}{3\sqrt{3}}\dfrac{1}{p_z}\dfrac{nEA}{L^3}(H^2 - B^2)^{3/2}, \\ r = \sqrt{(H^2 - B^2)/3}, \\ \theta = \theta_p, \\ z = 0, \end{cases} \qquad \begin{cases} \lambda = \dfrac{1}{3\sqrt{3}}\dfrac{1}{p_z}\dfrac{nEA}{L^3}(H^2 - B^2)^{3/2}, \\ r = \sqrt{(H^2 - B^2)/3}, \\ \theta = \theta_p + \pi, \\ z = 0. \end{cases} \tag{40a, b}$$

The tertiary branch belongs entirely to the surface of neutral equilibrium Ω_2, so it is totally composed of critical points. Considering that $V_2 \neq 0$, from (30b), these should be classified as limit points. Actually, λ is stationary along this branch since it is zero thoroughly.

5.3. Oblique load

Finally, we consider the general loading condition

$$p_r \neq 0 \quad \text{and} \quad p_z \neq 0. \tag{41a, b}$$

To discuss this case, we introduce the ratio

$$\mu = \frac{p_z}{p_r} \tag{42}$$

between the vertical and the radial components of the reference load vector, **p**. Thus, when $|\mu| \ll 1$ we have the case of a horizontal load with a small disturbing vertical load; vice versa, when $|1/\mu| \ll 1$, this load condition represents the case of a vertical load with a small disturbing radial load.

Due to the breakage of the axial symmetry, the solution is again expected to be dependent on the angle θ. Actually, the equilibrium equation (16) lead to the following solution

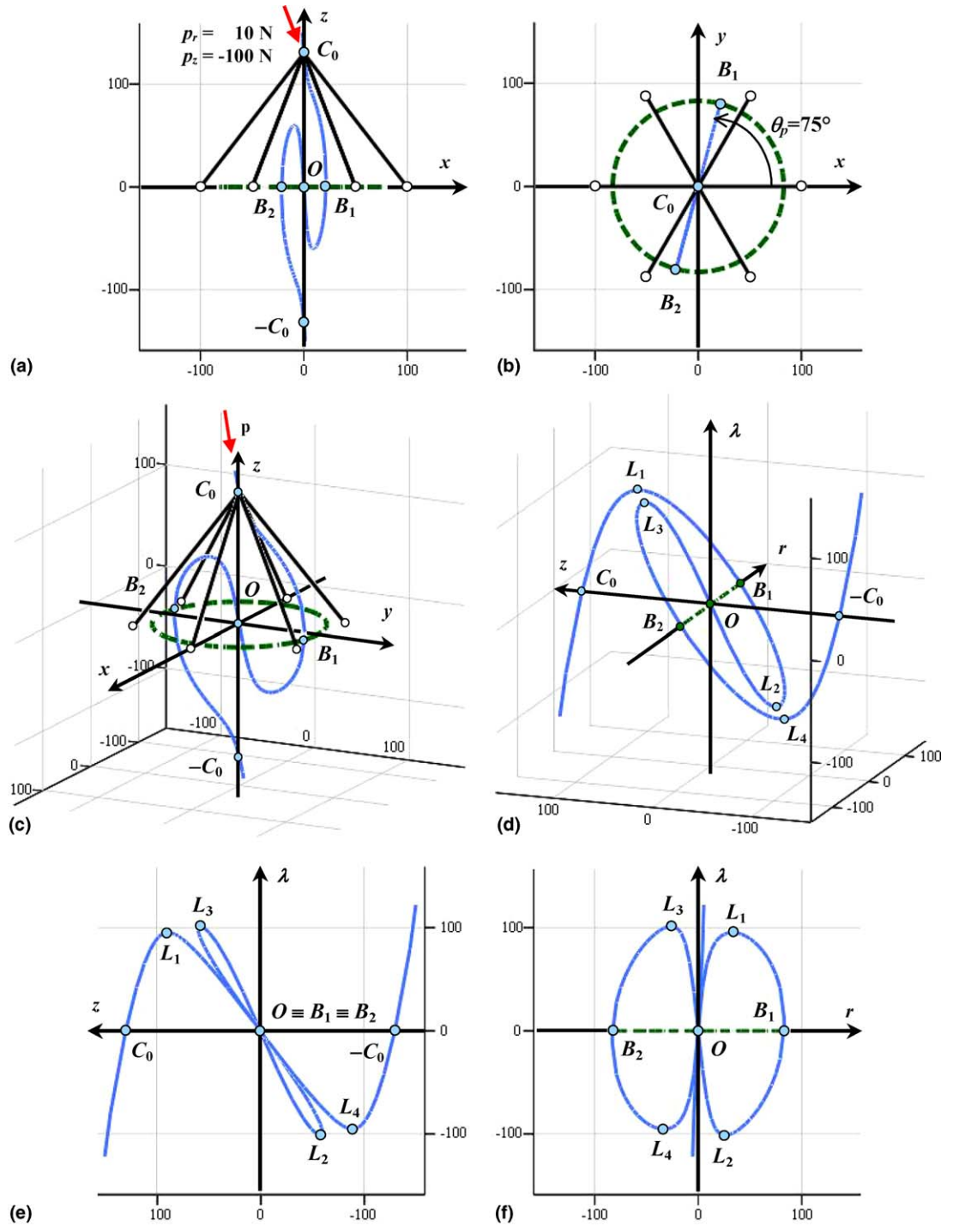

Fig. 9. Equilibrium path of the pyramidal truss subjected to an oblique load: (a) projection on the xz-plane, (b) projection on the xy-plane, (c) view in the xyz-space, (d) view in the $rz\lambda$-space, (e) projection on the $z\lambda$-plane, (f) projection on the $r\lambda$-plane.

$$\begin{cases} \lambda = \dfrac{1}{2}\dfrac{1}{p_r}\dfrac{nEA}{L^3} r(r^2 + z^2 - H^2 + B^2), \\ r \in [0, +\infty), \\ \theta = \theta_p, \\ z = \text{roots } [z^3 - \mu r z^2 - (H^2 - r^2)z + \mu r(H^2 - B^2 - r^2)], \end{cases} \quad \text{or} \tag{43a}$$

$$\begin{cases} \lambda = -\dfrac{1}{2}\dfrac{1}{p_r}\dfrac{nEA}{L^3} r(r^2 + z^2 - H^2 + B^2), \\ r \in [0, +\infty), \\ \theta = \theta_p + \pi, \\ z = \text{roots } [z^3 + \mu r z^2 - (H^2 - r^2)z - \mu r(H^2 - B^2 - r^2)], \end{cases} \tag{43b}$$

where 'roots' denotes the zeroes of the cubical polynomial in parentheses.

In *xyz*-space, (43a) and (43b) represent the *primary branch* of the equilibrium path, a unique curve lying in the vertical plane containing the *z*-axis and the direction of the reference load vector. The two expressions that compose the solution correspond to the two arcs of the curve lying in the half-planes $\theta = \theta_p$ and $\theta = \theta_p + \pi$, respectively, which are opposite with respect to the origin *O*. The path passes through the load-free equilibrium configurations (31a,b,c). Furthermore, if $H \geqslant B$, the equilibrium path is completed by a *secondary branch* given by the circle Γ_2. Some projections and views of the equilibrium path are plotted in Fig. 9, using the same numerical values considered before. The load is $p_r = 10$ N, $p_z = -100$ N, with $\theta_p = 75°$. The continuous curve represents the primary branch, while the dashed curve is the secondary one.

As in the previous cases, critical points are found at the intersections between the path and the neutral equilibrium surfaces. After some elementary algebra, we arrive at the following bi-quartic equation

$$r^8 + b_3 r^6 + b_2 r^4 + b_1 r^2 + b_0 = 0, \tag{44}$$

where

$$\begin{cases} b_0 = \dfrac{(H^2 - B^2)H^6}{3(\mu^2 + 1)^2}, \\ b_1 = -\dfrac{4(\mu^2 + 2)H^6 - 4(4\mu^2 + 1)H^4B^2 + 21\mu^2H^2B^4 - 9\mu^2B^6}{4(\mu^2 + 1)^2}, \\ b_2 = \dfrac{4(3\mu^2 + 4)H^4 - 4(12\mu^2 + 1)H^2B^2 + 39\mu^2B^4}{4(\mu^2 + 1)^2}, \\ b_3 = -\dfrac{10(\mu^2 + 1)H^2 - (33\mu^2 + 1)B^2}{3(\mu^2 + 1)^2}, \end{cases} \tag{45}$$

whose solutions furnish the *r*-coordinates of the requested critical points.

By discarding the physically meaningless imaginary solutions, we find that the primary branch intersects each of the neutral equilibrium surfaces in two points, thus giving rise to six critical points in all. The primary branch intersects the surface Ω_1 at the limit points L_1 and L_4, the surface Ω_2 at the bifurcation points B_1 and B_2, and, finally, the surface Ω_3 at the limit points L_2 and L_3.

6. Conclusions

The equilibrium stability problem for a wide class of elastic space trusses in the shape of a regular pyramid was posed. By assuming the joints to behave as ideal hinges and using the common hypotheses

of large nodal displacements, small or moderate deformation in bars and linear elastic material behaviour, a simple analytical model was formulated. Since these structures constitute the simplest three-dimensional generalisation of the planar von Mises truss, the aim of the analysis was that of verifying if a similar richness of post-critical responses could be observed also for the space model. The governing set of non-linear equilibrium equations was obtained by recourse to the principle of stationary total potential energy. The study of the conditions for stable equilibrium states led to the definition of three surfaces such that, when the top joint lies on them, the truss is in a state of neutral equilibrium. Regions of the coordinate space associated to stable equilibrium states were determined and the expressions of the eigenvectors associated to zero eigenvalues were derived, so the conditions for which bifurcation and/or snapping instability occur could be discussed. Furthermore, the configurations of the system where a state of equilibrium may take place in the absence of applied loads were analysed. Knowledge of the above configurations assumes a great importance in stability analysis, since they constitute points of obligatory passage for the equilibrium paths, irrespective of the reference load vector. The non-linear equilibrium problem was solved with reference to three different loading conditions. First, we considered a proportional vertical load acting on the top joint; then we analysed the case of a horizontal load; finally, we considered a load acting along a generic oblique direction. In each case, the presence of single or multiple critical points along the primary path, or along a complementary branch, was clearly identified; a deeper investigation was necessary to define the nature of each critical point and to establish the order they follow along the path. Complementary branches were also detected, where present.

Just as suspected, the solutions obtained confirm the great variety of the possible post-critical responses of the examined class of space trusses. Besides the well-known cases of primary and secondary branches, variously intersecting each other, very interesting cases of neutral equilibrium branches came out. The nature of these curves, entirely composed of critical points, was revealed. In particular, in the case of a vertical load, we found secondary branches made up entirely of bifurcation points, which together with the tertiary branches were able to generate a surface. Analogously, in the remaining two loading cases, we determined a complementary branch made up of limit points, where the load was identically zero. In our opinion, these branches result particularly hard to detect and trace by the standard numerical procedures of non-linear analysis, for which the given solutions may represent severe benchmark tests.

References

Bazant, Z.P., Cedolin, L., 1991. Stability of Structures: Elastic, Inelastic, Fracture, and Damage Theories. Oxford University Press, New York.

Crisfield, M.A., 1991. Non-linear finite element analysis of solids and structures. Essentials, Vol. 1. Wiley, Chichester.

Koiter, W.T., 1976. Current trends in the theory of buckling. In: Budiansky, B. (Ed.), Proceedings of the IUTAM Symposium on Buckling of Structures, Cambridge, MA. Springer-Verlag, Berlin, pp. 1–16.

Kouhia, R., Mikkola, M., 1989. Tracing the equilibrium path beyond simple critical points. International Journal for Numerical Methods in Engineering 28, 2923–2941.

Kouhia, R., Mikkola, M., 1999. Tracing the equilibrium path beyond compound critical points. International Journal for Numerical Methods in Engineering 46, 1049–1074.

Kumar, P., Pellegrino, S., 2000. Computation of kinematic paths and bifurcation points. International Journal of Solids and Structures 37, 7003–7027.

Ligarò, S., Valvo, P., 1999. A self-adaptive strategy for uniformly accurate tracing of the equilibrium paths of elastic reticulated structures. International Journal for Numerical Methods in Engineering 46, 783–804.

Pecknold, D.A., Ghaboussi, J., Healey, T.J., 1985. Snap-through and bifurcation in a simple structure. Journal of Engineering Mechanics 111 (7), 909–922.

Sewell, M.J., 1966. On the connection between stability and the shape of the equilibrium surface. Journal of the Mechanics and Physics of Solids 14, 203–230.

Sewell, M.J., 1968. A general theory of equilibrium paths through critical points. Proceedings of the Royal Society A 306, 201–238.

Tarnai, T., 2003. Zero stiffness elastic structures. International Journal of Mechanical Science 45, 425–431.

Thompson, J.M.T., Hunt, G.W., 1984. Elastic Instability Phenomena. John Wiley & Sons, New York.
von Mises, R., 1923. Über die Stabilitätsprobleme der Elastizitätstheorie. ZAMM 3, 406–422.
von Mises, R., Ratzersdorfer, J., 1925. Die Knicksicherheit von Fachwerken. ZAMM 5, 218–235.
Wempner, G.A., 1971. Discrete approximation related to non-linear theories of solids. International Journal of Solids and Structures 7, 1581–1599.